

# DEMONSTRATION AND OPTIMIZATION OF A DRIVE LASER FOR AN X-BAND PHOTOINJECTOR\*

D. J. Gibson<sup>†</sup>, S. G. Anderson, S. M. Betts, M. J. Messerly, H. H. Phan,  
M. Y. Shverdin, F. V. Hartemann, C. W. Siders, C. P. J. Barty,  
Lawrence Livermore National Laboratory, Livermore, CA 94550, USA

## Abstract

Recently, a drive laser for an S-band (2.86 GHz) rf photoinjector, designed to provide a pulse that has a flat temporal and spatial profile, has been built, commissioned, and put into service as part of the LLNL Compton-scattering monoenergetic  $\gamma$ -ray source program. This laser is based on an all-fiber oscillator and front-end amplification system, and provides both the laser light to generate the electrons as well as the rf signal that is amplified to accelerate them. Now, a new 11.424 GHz photoinjector is being developed, which has required a revised design for the laser system. The higher frequency has placed more stringent requirements on the synchronization stability, delivered pulse length, and pulse rise times to maintain the desired emittance. Presented here are the overall design and measured performance of the current system and a discussion of what changes are being made to address observed shortcomings and more demanding requirements to make the system ready for the next-generation Compton-scattering monoenergetic  $\gamma$ -ray source.

## INTRODUCTION

Compton-scattering systems, in which incoming high-intensity laser photons scatter off a relativistic electron beam, taking some of the electron energy, and emerge as high-energy  $\gamma$ -ray photons, have shown promise as a new class of light source. To operate with the best efficiency, it is important the electron beam used for the scattering have the highest possible brightness. Because the energy of the scattered photon depends on the angle between the scattering electron and the incoming laser beam, a high emittance translates directly into a broadening of the x-ray spectrum, degrading the  $\gamma$ -ray source performance. In order to produce the necessary high-brightness electron beams, we rely on photoinjector technology as an electron source, using a variant of the 1.6 cell BNL/SLAC/UCLA design[1]. We have built a fiber-based laser system designed to provide laser pulses that have a flat profile in space and time to minimize emittance[2]. This laser is detailed below.

## LASER OSCILLATOR AND AMPLIFIERS

The laser starts with the polarization-maintaining, fiber-based seed system. The passively mode-locked oscillator[3] feeds two systems, the photocathode drive laser described here and an interaction laser system for the scattering process. The oscillator generates 0.4 nJ pulses; their spectral bandwidth (shown in Fig. 1) is sufficient for 70 fs pulses. A feedback system keeps the oscillator pulse train locked to a 40.7785 MHz reference clock. After leaving the oscillator, the pulses are split in amplitude to seed the two systems mentioned above. This pulse train is also monitored with a photodiode to generate the accelerator rf, as discussed below.

Following the oscillator, a chirped fiber Bragg grating[4] narrows the spectrum to 8 nm and stretches the pulses to 3 ns. The loss through the stretcher is 18 dB; 6 dB of this is due to intentional spectral narrowing. The stretched pulses are amplified by a series of three micro-optic based Yb-doped fiber preamplifiers. The preamplifiers fibers have a mode diameter of 6  $\mu\text{m}$  and each preamp produces roughly 17 dB of gain. Accumulated amplified spontaneous emission (ASE) is stripped between stages in the spectral and time domains, the latter by acousto-optic modulators. The AOMs also reduce the pulse repetition rate to roughly 10 kHz to keep the average power from the preamplifiers modest as the pulse energy increases; the 10 kHz rate is high enough to prevent spontaneous Q-switching events. After the final fiber preamp, the pulse energy is roughly 1  $\mu\text{J}$ .

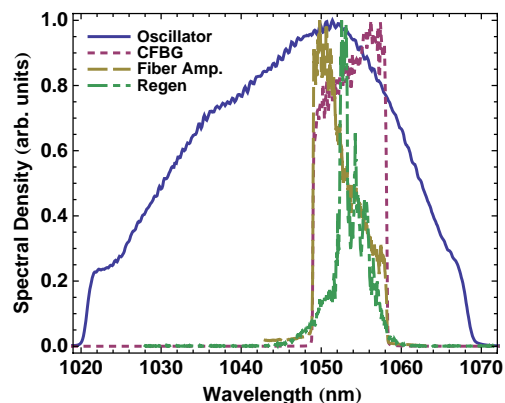


Figure 1: Laser spectra at the output of the oscillator, after the chirped fiber bragg grating, at the end of the fiber amplification stages, and after the regenerative amplifier.

\* This work performed under the auspices of the U.S. Department of Energy by Lawrence Livermore National Laboratory under Contract DE-AC52-07NA27344.

<sup>†</sup> gibson23@llnl.gov

The final fiber preamplifier is followed by a fiber amplifier based on a single-mode, single-polarization photonic crystal fiber having a mode diameter of  $29\ \mu\text{m}$  mode (Crystal Fibre PZ-41). This amplifier boosts the energy to  $30\ \mu\text{J}$  at 10 kHz.

The pulse energy is boosted by a regenerative amplifier based upon the design for the National Ignition Facility [5]. The amplifier head consists of a Nd:Phosphate glass (Schott LG770) rod that is end-pumped by an 800nm laser diode array homogenized by a hollow duct concentrator. The amplifier was designed to operate at 10 Hz with an 18 ns round trip time. The diode pump power and number of round trips were adjusted to yield 1.5 mJ output pulses at peak buildup for maximum energy stability. A Pockels cell enables Q-switched cavity-dumped operation.

Fig. 1 compares the spectra directly from the oscillator, after the CFBG stretcher, after the final amplifier, and after the regenerative amplifier. The gain of the Yb tilts the fiber amplifier spectra, and the regenerative amplifier narrows the spectrum and increases the pulse width limit to roughly 0.6 ps. Because we want to get  $< 0.24$  ps pulses, we plan to switch to an all-fiber amplification chain. Currently we are limited by nonlinear effects in the fibers. By adding an intermediate amplifier with an  $11\ \mu\text{m}$  core and a final amplifier stage with an  $85\ \mu\text{m}$  core, we expect to be able to get up to 1 mJ out of the fiber system at 10 kHz.

## RF GENERATION

Precision electron beam generation requires the laser arrival time at the photocathode be synchronized to within  $1^\circ$  of phase to the accelerating rf in the photoinjector cavity; thus, the two systems must be locked to the same clock. As mentioned above, the laser is locked to a 40.7785 MHz reference crystal oscillator, the 70th subharmonic of the accelerator's 2.8545 GHz operating frequency. The laser photodiode signal, used to keep the laser locked to the master crystal and to generate the timing triggers for all the laser and accelerator systems, is also filtered to produce a sinusoidal rf signal that tracks the laser pulse train even if it drifts from the reference frequency. This signal is fed into a phase-locked coaxial resonant oscillator which puts out S-band rf phase-locked to the laser pulse train.

Measurement of the phase noise showed jitter in the rf timing of 0.6 ps at frequencies above 1 kHz. For an S-band system, where  $1^\circ$  of rf phase is 0.97 ps, this is sufficient. However, for an X-band system where  $1^\circ = 0.24$  ps, this jitter is too high. For the upgraded X-band system, we will try both the method described above with better components as well as using a 12 GHz photodiode to produce the 11.424 GHz harmonic signal directly from the short pulse. Measurements of the jitter between the rf phase in the gun and the laser arrival at the cathode will determine which scheme provides optimal stability.

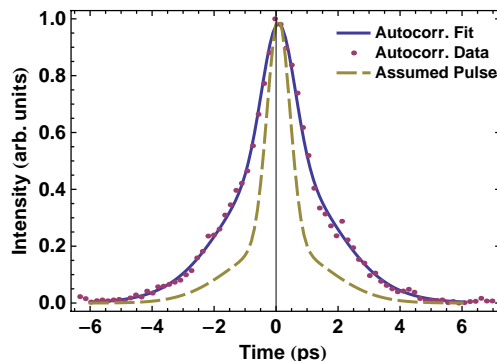


Figure 2: The autocorrelation of the compressed IR pulse, including a fit to the data and the pulse shape that matches that fit.

## LASER SHAPING

Following the regenerative amplifier, the pulse is recompressed with a transmission efficiency of 66%. The compressor grating is a 1740 l/mm dielectric grating at an incidence angle of  $75^\circ$ , with a translatable horizontal roof mirror to set the effective grating separation and a vertical roof mirror to offset the beam for extraction at the compressor exit. Fig. 2 shows an autocorrelation measurement of the laser pulse. Assuming a gaussian pulse shape with a gaussian pedestal, fitting the autocorrelation finds that the measurement is consistent with a 0.87 ps FWHM pulse sitting on a 3.6 ps FWHM pedestal containing 20% of the total energy.

Since the goal is to illuminate Cu or Mg cathodes, photon energies above the Cu work function are required. The 1053 nm laser light is frequency doubled to 527 nm with a 1.0 mm thick BBO crystal, then doubled again to 263 nm with a 0.45 mm thick BBO crystal, yielding a final energy of  $100\ \mu\text{J}$ .

To approximate the desired temporal shape of the laser pulse, we stack several short pulses together to minimize the rise and fall times of the beam while maintaining the desired 16 ps overall pulse length. The frequency-quadrupled pulse is fed into a hyper-Michelson pulse stacker [6], which splits the pulse into 16 replicas through a series of four beam splitters. By sequencing the beam splitters correctly (using the two outputs of the first as two inputs to the second, etc.), rotating the polarization of one of the two final outputs with a waveplate, then combining the two outputs with a polarizer, no laser energy is wasted. Choosing the delays correctly allows adjacent pulses to have crossed polarizations, minimizing interference between the pulses which could lead to significant longitudinal ripple on the delivered pulse. Because we are illuminating the photocathode nearly on axis, the polarization of the laser light isn't significant.

The resulting temporal profile was measured two ways. First, the output of the stacker ( $4\omega$ ) was cross-correlated with the residual IR light ( $1\omega$ ) from the frequency conversion in a BBO crystal, resulting via difference frequency

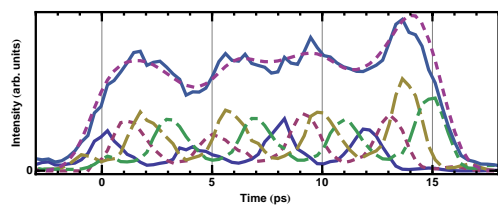


Figure 3: The crosscorrelation of the compressed IR pulse with the stacked UV pulses and the summed profile. See text for details

generation in a signal at  $3\omega$ . The pulses were measured in groups of four so they could be seen individually, and the results are shown at the bottom of Fig. 3. The gaussian width of the individual pulses is  $\sigma = 0.83$  ps. Given the assumed shape of the IR pulse from the autocorrelation, this width is consistent with a UV pulse width of 750 fs FWHM. Second, at the output of the hyper-Michelson stacker, the energy of each of the individual pulses was measured by selectively blocking the delay arms. Using this set of energies, coupled with the width measured in the cross-correlation, to define gaussian pulses to sum, the expected pulse shape is shown in the upper plot of Fig. 3 (dashed line). Scaling the cross correlation measurements based on the measured energy of the largest pulse in each group, then summing those four plots, we obtain the curve shown in the upper plot of Fig. 3 (solid line). The deviation from the target flat-topped shape is due to the uneven splitting ratio of the beamsplitters used — measurement of the transmission of each of the splitters predicts the energy distribution observed. This issue will be corrected in the X-band version of the system.

To get the required transverse beam shape, the output of the hyper-Michelson stacker is clipped by a 1.2 mm diameter aperture. Although this method has the disadvantage of discarding a significant amount of laser light, it has the advantages of being both simple to implement and easy to modify (to allow optimization of the electron emittance). The gaussian beam size at the aperture is measured to be  $\sigma_x = 0.61$  mm  $\times$   $\sigma_y = 0.87$  mm, which means the 1.2 mm diameter aperture will pass only 28% of the laser energy. The aperture plane is relay imaged with a pair of 1 m focal length lenses, forming a 1:1 imaging telescope, to the cathode surface in the photoinjector. A small portion of the beam is picked off and sent to a camera sitting at an equivalent image plane (Fig. 4) and an energy meter. The energy delivered to the photocathode is adjusted to get the desired operating charge, but a value of  $17 \pm 1$   $\mu$ J is typical.

## CONCLUSIONS

We have built and demonstrated a laser designed to drive a photoinjector and generate high-brightness beams. Using this laser pulse, an emittance of 1.8 mm mrad at 0.8 nC and 5.5 MeV was measured out of the photoinjector[7]. We are now developing an X-band accelerator and plan to

[Accelerator Technology - Subsystems](#)

[T24 - Lasers](#)

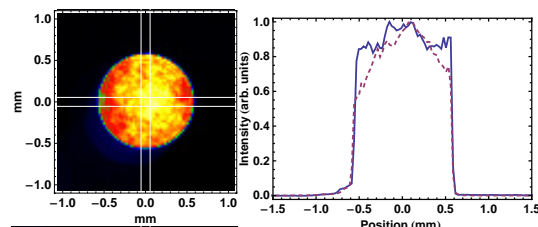


Figure 4: The apertured laser profile and lineouts along the horizontal and vertical axes

refine this laser system further, by eliminating the regenerative amplifier and improving the pulse stacking, to achieve the faster rise times, shorter overall pulse length, and more stringent jitter specs that the 4x increase in frequency (and commensurate 4x decrease in sizes) the switch imposes.

## REFERENCES

- [1] S. G. Anderson, et al., "Commissioning of a High-Brightness Photoinjector for Compton Scattering X-Ray Sources", PAC'07, Albuquerque, May 2007, TUPMS028, p. 1242 (2007).
- [2] D. J. Gibson, et al., "Numerical Optimization of Electron Beams for High Brightness x- and  $\gamma$ -Ray Production", Adv. Accel. Concepts, 12th Workshop, AIP Conf. Proc. 877, 602 (2006).
- [3] H. Lim, F. Ilday, and F. Wise, "Generation of 2-nJ pulses from a femtosecond ytterbium fiber laser," Opt. Lett. 28, 660-662 (2003).
- [4] M. Durkin, M. Ibsen, M. J. Cole, R. I. Laming, "1 m long continuously-written fibre Bragg gratings for combined second- and third-order dispersion compensation," Elect. Lett., 33, 1891-1893, (1997).
- [5] M. Bowers, et al., "The injection laser system on the National Ignition Facility", Proc. SPIE, 6451, 1M (2007).
- [6] C. W. Siders, et al., "Efficient High-Energy Pulse-Train Generation Using a 2 n -Pulse Michelson Interferometer", Appl. Opt. 37, 5302 (1998).
- [7] S. G. Anderson, et al., "Observation of Nonlinear Space-Charge Induced Phase Space Wave-Breaking and Emittance Growth in a High-Brightness Photoinjector", these proceedings (2009).